Graefes Arch Clin Exp Ophthalmol
DOI 10.1007/s00417-015-3254-1

RETINAL DISORDERS

En face OCT in Stargardt disease

Andrea Sodi[1] · Dario Pasquale Mucciolo[1] · Francesca Cipollini[1] · Vittoria Murro[1] · Orsola Caporossi[1] · Gianni Virgili[1] · Stanislao Rizzo[1]

Received: 6 August 2015 / Revised: 15 December 2015 / Accepted: 21 December 2015

Abstract
Purpose To evaluate the structural features of the macular region by enface OCT imaging in patients with clinical diagnosis of Stargardt disease, confirmed by the detection of *ABCA4* mutations.
Methods Thirty-two STGD patients were included in the study for a total of 64 eyes. All patients received a comprehensive ophthalmological examination, color fundus photography, fundus auto-fluorescence imaging and OCT. Five OCT scans were considered: ILM and RPE scans (both automatically obtained from the instrument), above-RPE slab, photoreceptor slab and sub-RPE slab (these last three manually obtained).
Results ILM scans showed evident radial folds on the retinal surface in 8/64 eyes (12.5 %). In 6 of the 7 patients, these vitreo–retinal interface abnormalities were unilateral. The photoreceptor slab showed some macular alterations ranging from dis-homogeneous, hypo-reflective abnormalities (7/64 eyes, 11 %) to a homogeneous, well-defined, roundish, hypo-reflective area (17/64 eyes, 27 %) in all the eyes. The sub-RPE slab showed a centrally evident, hyper-reflective abnormality in 58/64 eyes (90.6 %). Superimposing the sub-RPE slab over the images corresponding to the photoreceptor slab, the area of the photoreceptor atrophy sharply exceeded that of the RPE atrophy (44/46 eyes, 96 %).
Conclusion Enface OCT proved to be a clinically useful tool for the management of STGD patients, illustrating in vivo the structural abnormalities of the different retinal layers.

✉ Dario Pasquale Mucciolo
dario.mucciolo@gmail.com

[1] Careggi Teaching Hospital , Eye Clinic, University of Florence, Largo Brambilla 3, 50134 Florence, Italy

Keyword Maculopathy · Stargardt · OCT · Photoreceptors · Retina · Dystrophy

Introduction

Stargardt disease (STGD) is the most common inherited form of macular degeneration with a prevalence of about 1:10000. It is characterized by progressive macular atrophy. Sometimes the disease can spread beyond the posterior pole to retinal periphery determining diffused retinal degeneration. STGD onset is usually in childhood or young adulthood with a later progressive worsening of the clinical picture. Visual acuity reduction with central scotoma is the main symptom. On fundus examination, macular atrophy is often associated with typical fishtail, white–yellowish spots (flecks) at the posterior pole and sometimes at the retinal mid-periphery [1]. Fundus auto-fluorescence imaging may show macular hypo-autofluorescence, hyper–hypo-autofluorescent flecks and hyper-autofluorescent perimacular rings [2], while OCT scans show a reduction of foveal thickness and a disruption/disappearance of the photoreceptor layer [3]. Electroretinogram (ERG) abnormalities can be recorded in different stages of the disease [4, 5].

STGD has been associated with mutations in the *ABCA4* gene, encoding a specific transport protein of the retina, expressed exclusively at the level of the outer segment of the photoreceptors [6, 7]. Impaired function of this protein leads to the accumulation of lipofuscins and their derivatives within the retinal pigment epithelium (RPE), with consequent RPE degeneration and photoreceptor disruption [8, 9]. The sequence of atrophy has not been completely clarified, and, in particular, we do not know for sure whether the RPE or the photoreceptors degenerate first.

Published online: 07 January 2016

In recent years, the development of molecular biology and the first clinical trials of gene therapy have offered new chances for STGD patients, stimulating research towards better evaluation of the morphological and functional features of STGD [10, 11]. A better visualization of retinal structures could be very useful to understand the physiopathology of the disease and to monitor its progression and its possible response to innovative treatment.

En face optical coherence tomography (ef-OCT) can provide data with an overview of transversal slices at any different depth through the retina, not available in conventional longitudinal OCT scans [12–20]. Nowadays, there is only limited information about ef-OCT examination in STGD [21]. In the present study, we report on the structural features of eyes with clinical diagnosis of STGD confirmed by the detection of *ABCA4* mutations.

Methods

Study population

Thirty-two patients with a clinical diagnosis of STGD were included in the study. STGD patients were recruited through the Referring Center for Inherited Retinal Degeneration of the Eye Clinic, Careggi Teaching Hospital, Florence, Italy from January 2013 to January 2014.

Criteria for STGD phenotype included the following: appearance in the first or second decade of life; bilateral progressive central vision loss; macular atrophy/dystrophy; normal caliber of retinal vessels; absence of pigmented bone spicules; normal or mildly abnormal full-field ERG. Fluorescein angiography was performed only in a small number of the patients because, in most cases, it was not clinically helpful for the diagnosis. Exclusion criteria were: refractive errors (>± 5 diopters [D], spherical equivalent), significant cataract or other media opacities, ocular diseases other than STGD, age <15 or >50 years at the moment of diagnosis, and previous photorefractive treatment. Moreover, our patients did not show any significant systemic diseases and none of them had a family history of other inherited retinal or systemic disorders.

Thirty patients carried at least two mutations of the gene *ABCA4*. Two patients carried only one *ABCA4* mutation, but they were still included in the study because their clinical picture was typical of STGD (Table 1).

Ophthalmological examination

All the patients included in the study first received a comprehensive ophthalmological examination including measurement of visual acuity with ETDRS charts, evaluation of intraocular pressure with applanation tonometry, biomicroscopy of the anterior segment and fundoscopy after dilation with tropicamide 1 % eye drops.

Fundus imaging

After the ophthalmological examination, all the patients underwent color fundus photography, fundus autofluorescence imaging and OCT. Color fundus photographs of the posterior pole and the surrounding areas of both eyes were taken using a fundus camera with a 45° field of vision centered on the macula (FF450 Retinograph, Carl Zeiss Meditec, Jena, Germany). Fundus auto-fluorescence (FAF) imaging was performed with a confocal scanning laser ophthalmoscope (Heidelberg Retina Angiograph 2; Heidelberg Engineering, Dossenheim, Germany) using a 30° field of vision at a resolution of 1536 × 1536 pixels. Spectral domain (SD)-OCT scans were obtained with a Cirrus Spectral Domain OCT (Carl Zeiss Meditec Inc., Dublin, CA, USA). The acquisition protocol consisted of a macular cube 512 × 128 scan pattern in which a 6.0 × 6.0-mm region of the retina was scanned (a total of 65,536 sampled points) within a scan time of 2.4 seconds. After image acquisition, those with a signal strength of ≤8 were excluded. The SD-OCT data were processed through the Advanced Visualization Analysis software, obtaining OCT scans at different depths in the retina. Image processing was performed by three experienced operators (VM, OC, and DPM) who shared all the procedures.

Two scans automatically provided by the instrument software, through a specific algorithm of the cube scan analysis, were considered:

- **Inner limiting membrane (ILM) scan**: exploring the retinal surface and then the possible abnormalities of the vitreo–retinal interface (Fig. 1)
- **RPE scan**: exploring the RPE layer (Fig. 1).

  We then analyzed three other slabs, obtained with reference to the RPE fit, which is a representation of the RPE fitted for each specific eye based on the retina's overall curvature. These slabs are outlined adjusting the parameters of thickness and depth of the retinal slices, tailored to provide information about specific retinal structures with significant clinical implications:
- **Photoreceptor slab:** image data from a 10-μm slab, manually positioned on the photoreceptor layer, detected in the outer retina [19] in the region above the RPE segmentation line. The photoreceptor layer was identified as the hyper-reflective band probably corresponding to the ellipsoid zone, or the photoreceptor inner segment [22]. The ellipsoid zone could be considered a significant marker of the photoreceptors presence and integrity even if it does not image the complete structure of the photoreceptors but only a part of them. We used a slice thinner than the one previously suggested [19] because it was

Table 1 Clinical and molecular data of STGD patients. *BCVA* best corrected visual acuity

ID	Age (ys)	Onset (ys)	Sex	BCVA OD logMAR	BCVA OS logMAR	Fundus appearance	Mutation 1	Mutation 2	Mutation 3
1	14	13	M	1	1	Macular distrophy	c.2345 T > A (p.Trp782*)	c.3089 T > A (p.Leu1030Gln)	
2	36	33	F	0,2	0,1	Macular distrophy	c.5882G > A (p.Gly1961Glu)	c.1035_1036delinsAT (p.Tyr345*)	
3	11	10	F	0,7	1	Macular distrophy	c.2888G > T (p.Gly963Val)	c.6449G > A (p.Cys2150Tyr)	
4	37	8	F	1	1	Macular RPE atrophy with flecks inside vascular arcades	c.5882G > A (p.Gly1961Glu)	c.571-2A > T	
5	36	26	F	0,7	0,7	Macular RPE atrophy with flecks inside vascular arcades	c.1714C > T (p.Arg572*)	c.4417C > A (p.Leu1473Met)	c.5882G > A (p.Gly1961Glu)
6	53	12	F	1,3	1,3	Macular RPE atrophy with flecks inside vascular arcades	c.5882G > A (p.Gly1961Glu)	c.1245C > A (p.Asn415Lys)	
7	50	42	F	1	1	Macular RPE atrophy with flecks inside vascular arcades	c.5882G > A (p.Gly1961Glu)	c.3056C > T (p.T1hr019Met)	
8	43	14	M	0,7	0,7	Macular RPE atrophy with flecks inside vascular arcades	c.5882G > A (p.Gly1961Glu)	c.3531C > A (p.Cys1177*)	
9	21	17	F	1	1	Macular RPE atrophy with flecks inside vascular arcades	c.5196 + 1G > A	WT	
10	26	17	F	1	1	Macular RPE atrophy with flecks inside vascular arcades	c.2461 T > A (p.Trp821Arg)	c.3323G > A (p.Arg1108His)	c.4297G > A (p.Val1433Ile)
11	34	32	M	1	0,7	Macular RPE atrophy with flecks inside vascular arcades	c.4667 + 1G > A	c.5882G > A (p.Gly1961Glu)	
12	36	31	F	0,4	0,2	Macular RPE atrophy with flecks inside vascular arcades	c.286A > G (p.Asn96Asp)	c.5882G > A (p.Gly1961Glu)	
13	31	23	F	0,4	0,7	Macular RPE atrophy with flecks inside vascular arcades	c.6537del (p.Pro2180Leufs*3)	WT	
14	31	12	F	1	1	Macular RPE atrophy with flecks inside vascular arcades	c.2791G > A (p.Val931Met)	c.4234C > T (p.Gln1412*)	
15	69	38	F	1,3	1,3	Macular RPE atrophy with flecks inside vascular arcades	c.5882G > A (p.Gly1961Glu)	c.571-2A > T	
16	28	17	F	1	1	Macular RPE atrophy with flecks beyond vascular arcades	c.4667 + 1G > A	c. 5512C > A(p.His1838Asn)	
17	56	29	M	1	1	Macular RPE atrophy with flecks beyond vascular arcades	c.2461 T > A (p.Trp821Arg)	c.4128G > A (p.=) *(p.Gln1376Gln)*	
18	68	45	F	1,6	0,1	Macular RPE atrophy with flecks beyond vascular arcades	c.1714C > T(p.Arg572*)	c.4417C > A (p.Leu1473Met)	
19	50	20	M	1	1	Macular RPE atrophy with flecks beyond vascular arcades	c.4919G > A (p.Arg1640Glu)	c.6446G > T (p.Arg2149Leu)	
20	34	19	F	1	1	Macular RPE atrophy with flecks beyond vascular arcades	c.768G > T (p.Val256Val)	c5714 + 5G > A	
21	16	10	M	0,7	0,7	Macular RPE atrophy with flecks beyond vascular arcades	c.4253 + 6C > T	c.4352 + 1G > A	c.5692C > T (p.Arg1898Cys)
22	18	14	M	0,2	0,7	Macular RPE atrophy with no flecks	c.288C > A (p.Asn96Lys)	c.2791G > A (p.Val931Met)	c.5882G > A (p.Gly1961Glu)
23	18	14	M	0,4	0,1	Macular RPE atrophy with no flecks	c.288C > A (p.Asn96Lys)	c.2791G > A (p.Val931Met)	c.5882G > A (p.Gly1961Glu)
24	49	10	F	1,3	1,3	Macular RPE atrophy with no flecks	c.5882G > A (p.Gly1961Glu)	c.5417G > A (p.Ser1806Asn)	
25	51	25	M	1	1	Macular RPE atrophy with no flecks	c.2461 T > A (p.Trp821Arg)	c.5882G > A (p.Gly1961Glu)	
26	15	5	M	1	1	Macular RPE atrophy with no flecks	c.1622 T > C (p.Leu541Pro)	c.3113C > T (p.Ala1038Val)	c.2105 T > C (p.Leu702Pro)
27	25	8	F	1,6	1,3	diffuse RPE atrophy	c.571-2A > T	c.2743G > A (p.Asp915Asn)	
28	23	12	F	0,7	1	Diffuse RPE atrophy	c.5018 + 2 T > C	c.5898 + 5del	
29	24	10	M	1	1	Diffuse RPE atrophy	c.5018 + 2 T > C	c.5898 + 5del	
30	65	9	F	hm	lp	Diffuse RPE atrophy	c.2887G > C (p.Gly963Arg)	c.5714 + 5G > A	
31	42	10	F	1,3	1,3	Diffuse RPE atrophy	c.5714 + 5G > A	c.5917del (p.Val1973*)	
32	29	10	M	1	1	Diffuse RPE atrophy	c.571-2A > T	c.571-2A > T	

able to show a better focalization of the layer of interest. Moreover, the contiguous structures could be better evaluated in the following slab. (Fig. 2)

– **Above-RPE slab**: image data from a 20-μm slab, manually positioned just above the RPE fit level. This slice aims to visualize the inward protrusion of the RPE

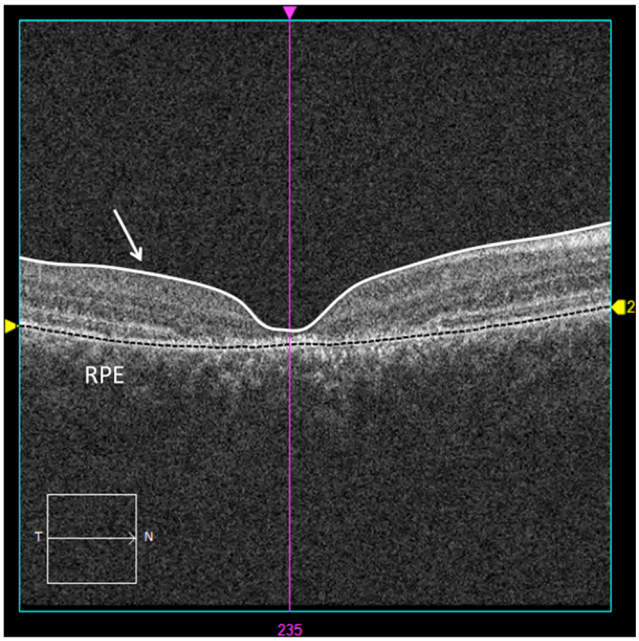

Fig. 1 ILM scan pointed out by a white line (*arrow*) and RPE scan underlined by a *black dash*; these are scans automatically provided by the instrument software through a specific algorithm of the cube scan analysis;

surface, and then in STGD, it should show better imaging of the flecks. The latter usually corresponds to focal RPE thickening due to abnormal lipofuscin accumulation. (Fig. 3)

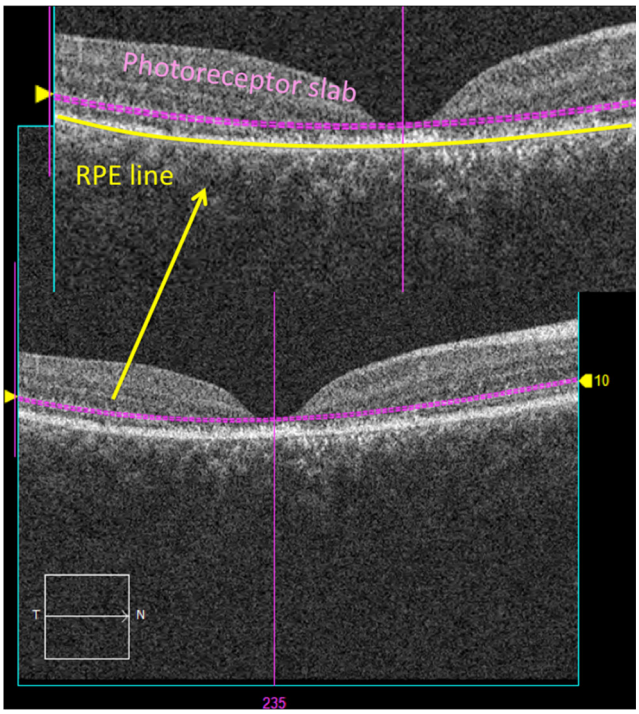

Fig. 2 Photoreceptor slab, image data from a 10-μm slab, *violet lines* manually positioned on the ellipsoid zone (IS/OS), detected in the outer retina in the region above the RPE segmentation line (*yellow line*);

– **Sub-RPE slab**: image data from 65 μm to 400 μm below the RPE fit level. This approach uses the light penetrating below the RPE into the choroid and sclera, allowing an optimal visualization of the areas of RPE atrophy [19, 23]. (Fig. 4)

For each patient, the ef-OCT images obtained with the described procedures were carefully analyzed showing the prevalence of the different morphological patterns. Even if STGD usually has a symmetrical evolution in the two eyes, this may not be true in all cases, and, therefore, each eye of the same patient was considered separately for analysis. Ef-OCT scans were then compared to the corresponding color fundus photographs and auto-fluorescence images.

Results

The group of patients included in the study consisted of 32 patients (12 males and 20 females, average age 36 yrs., range 11–50 yrs.), for a total of 64 eyes. Visual acuity was very variable, ranging from bare light perception to 20/25. Ophthalmoscopy showed only an abnormal macular reflex in one patient, flecks at the posterior pole with mild RPE abnormalities in 2 patients, macular atrophy with flecks at the posterior pole in 12 patients, macular atrophy with flecks spread beyond the vascular arcades in 6 patients, macular

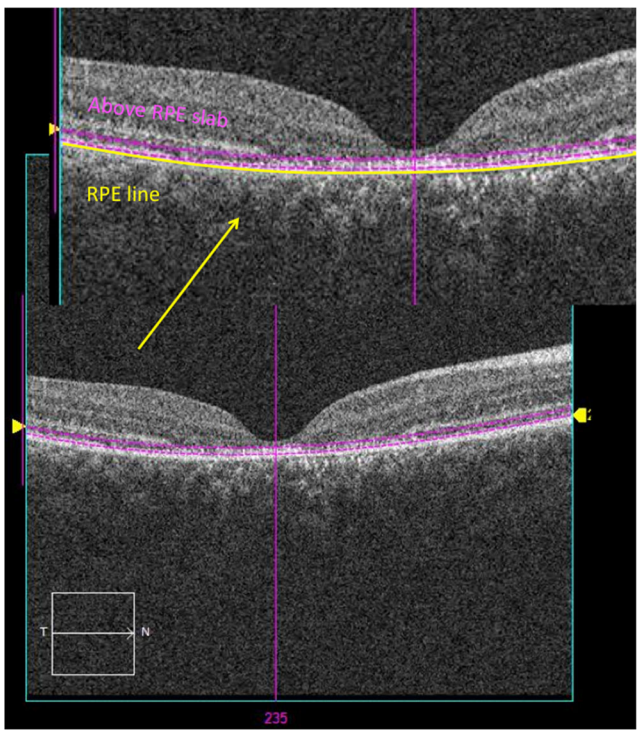

Fig. 3 Above-RPE slab, image data from a 20-μm slab, *violet lines* manually positioned just above the RPE fit level (*yellow line*);

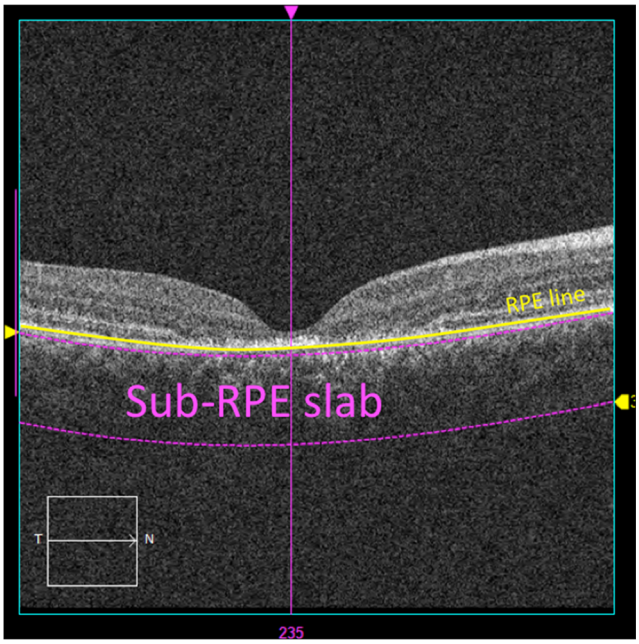

Fig. 4 Sub-RPE slab, image data from 65 μm to 400 μm, *violet lines* below the RPE fit level.

atrophy without flecks in 5 patients and diffused chorioretinal atrophy in 6 patients. Auto-fluorescence images were consistent with funduscopic findings, with better evidence of RPE disappearance in cases of macular atrophy. Twenty-six patients showed a central scotoma of variable size while 6 patients (corresponding to those with diffused chorioretinal atrophy) also presented para-central and peripheral losses.

ILM scans showed a normal appearance in 25 patients (50/64 eyes, 78,1 %) while 8 eyes of 7 patients (8/64, 12.5 %) showed some vitreo–retinal interface abnormalities with evident radial folds of the inner limiting membrane (Fig 5 a,b) [14]. Among the eyes with ILM abnormalities, 5 eyes were characterized by diffused RPE dystrophy, while in 3 eyes macular RPE atrophy and flecks could be found. The visual acuity in 7 eyes was 20/200, while in one eye it was limited to bare light perception.

Fig. 6 RPE scan of the left eye of a 49-year-old STGD patient showing a roundish dis-homogeneous central hypo-reflective area; severe RPE atrophy was detected at fundus examination and BCVA was 20/125

RPE scans did not show significant abnormalities in 39 eyes while in the other 25 (25/64 eyes, 39 %) it was possible to detect a more or less homogeneous roundish hypo-reflective area (Fig. 6)

The photoreceptor slab showed some macular alterations in all the eyes, ranging from dis-homogeneous hypo-reflective abnormalities (4 patients, 7/64 eyes, 11 %; Fig. 7a) to a homogeneous, well-defined, roundish, hypo-reflective area which could be observed in 10 patients (17/64 eyes, 27 %; Fig.7b). In 22 patients (40/64 eyes, 63 %), some hyper-reflective alterations could be found at the center of a larger, hypo-reflective area (Fig. 7c).

With the above-RPE slabs, 5 patients (9/64 eyes, 14 %) showed a central, dis-homogeneous, hypo-reflective area, while 12 patients (23/64 eyes, 36 %) presented at the posterior pole showed a hypo-reflective alteration including some central hyper-reflective structures (Fig. 8a). In two cases, these hyper-reflective structures assumed a radial disposition with a "spoke-like" appearance (Fig.8b). In almost half of the

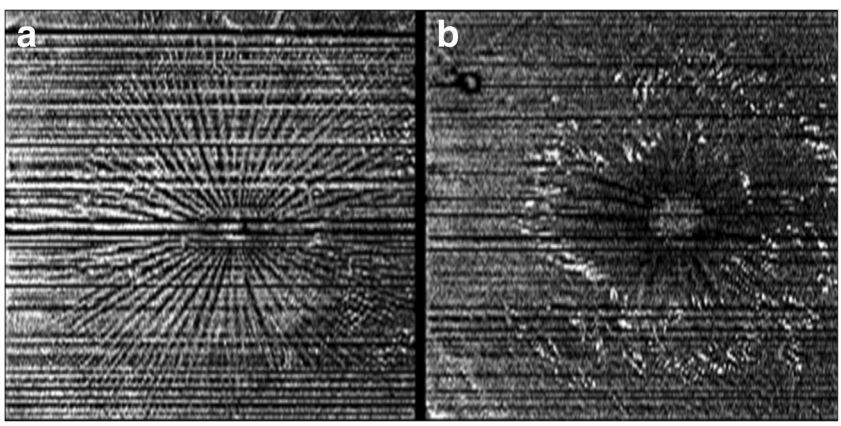

Fig 5 (**a**, **b**) ILM scan of two STGD patients showing radial folds of the retinal surface; **a**) left eye of a male patient, 30 years old with a BCVA of 20/200, **b**) left eye of a female patient, 26 years old, BCVA of 20/200

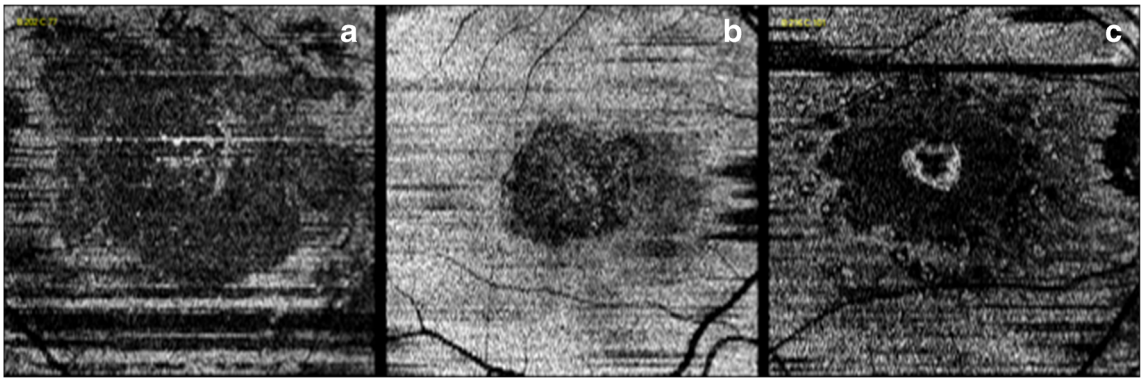

Fig. 7 (**a**, **b**, **c**) Photoreceptor slab scan showing central, dis-homogeneous, hypo-reflective abnormalities in the left eye of a 35-year-old STGD patient with a BCVA of 20/200 (**a**); a roundish, dis-homogeneous, central, hypo-reflective area in the right eye of a 19-year-old STGD patient with a BCVA of 20/63 (**b**); some irregular hyper-reflective abnormalities in the middle of the hypo-reflective area in the right eye of a 54-year-old STGD patient with a BCVA of 20/200(**c**)

patients (31/64, 48,4 %), the hypo-reflective central area was surrounded by some hyper-reflective alterations (Fig. 8c). In one eye, it was possible to observe a continuous hyper-reflective halo at the border of the central hypo-reflective area (Fig. 8d).

The sub-RPE slab showed in 29 patients (58/64 eyes, 90.6 %) a centrally evident, hyper-reflective abnormality determined by the light penetrating into the choroid through the disruption and atrophy of the overlying RPE (Fig. 9).

In the patients (46/64 eyes, 72 %) where the contrast of the image and the shape of atrophic alterations allowed a reliable measurement, we superimposed the sub-RPE slab over the images corresponding to the photoreceptor slab of the same OCT scan. In this way, we compared the area of atrophy in both images (Fig. 10). Three experienced operators (VM, OC, and DPM) performed subjective evaluation of comparative atrophy extension. They unanimously stated that in 44/46 eyes

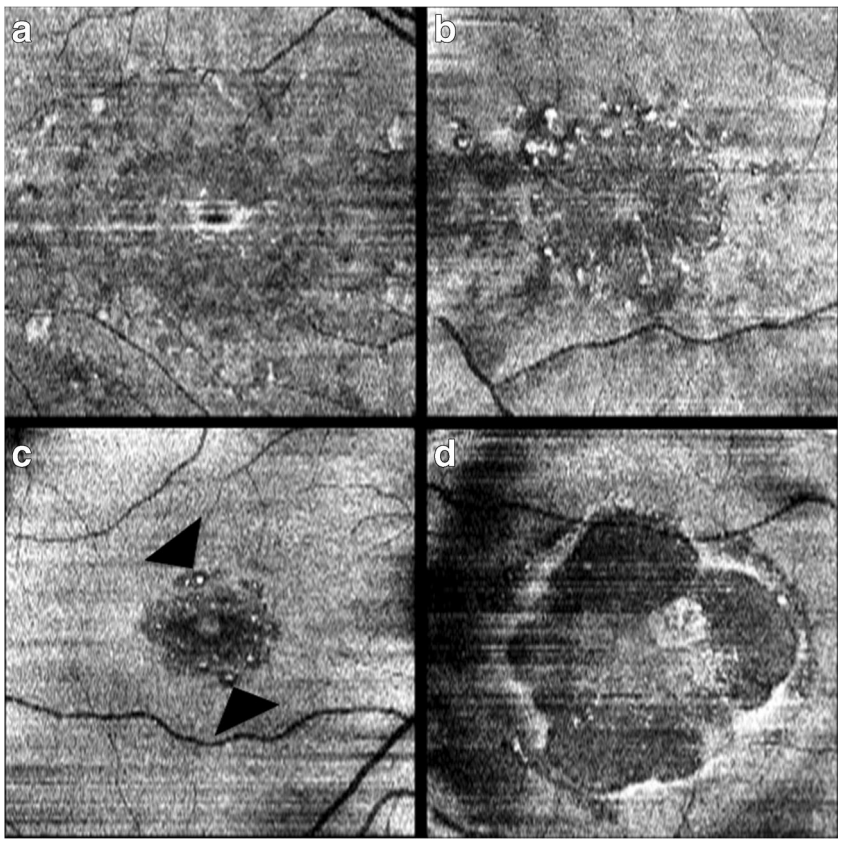

Fig. 8 (**a**, **b**, **c**, **d**): The above-RPE slab shows in the left eye of a female patient, 17 years old, a central hypo-reflective area with some internal, irregular, hyper-reflective structures, BCVA was 20/200. This pattern is present in most of the STGD patients (**a**). In the left eye of a female patient, 37 years old, the hyper-reflective structures presented a radial, spoke-like appearance, BVCA was 20/32 (**b**). Hyper-reflective structures (*arrowheads*) surrounding the hypo-reflective central area in the right eye of a female patient, 33 years old, BCVA of 20/32 (**c**). In the left eye of a female patient, 49 years old, there is a continuous hyper-reflective halo at the border of the central hypo-reflective area, BCVA was 20/125 (**d**)

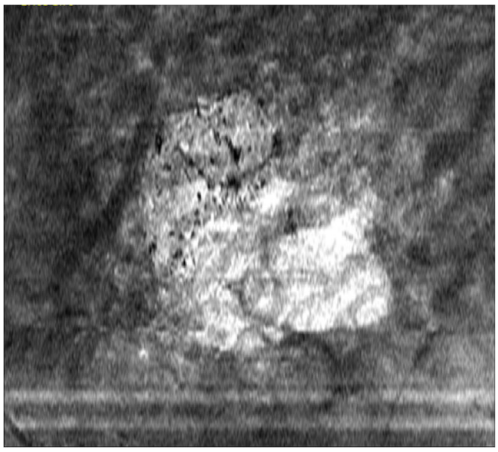

Fig. 9 Sub-RPE slab showing in a STGD, 57-year-old, male patient with BVCA of 20/200 a centrally evident, hyper-reflective abnormality corresponding to macular atrophy

(96 %) the area of photoreceptor atrophy sharply exceeded that of RPE atrophy, while in one patient (2/46 eyes, 4 %), the area of RPE atrophy was as large as the hypo-reflective area of the photoreceptor slab.

Discussion

The ef-OCT scans of a group of STGD patients were evaluated. In all the patients, signal strength was higher or equal to 8/10. For each eye, five different visualization modalities were considered: ILM scan, photoreceptor slab, above-RPE slab, RPE scan, sub-RPE slab.

ILM scans showed evident radial folds or retinal alterations of the surface in 8/64 eyes (12.5 %). In most of the cases (6/7 patients), these vitreo–retinal interface abnormalities were unilateral and, moreover, they were probably unrelated to a specific genotype and more likely due to local factors. Furthermore, they could even be seen in young patients with relatively recent onset of the macular disorder and, therefore, they were probably not associated with age or duration of the disease. We have already reported on a case of unilateral epiretinal membrane in association with STGD [24] and in recent years a high prevalence of vitreo-retinal interface abnormalities has been reported in association with retinitis pigmentosa (RP), a retinal dystrophy with pathogenic and clinical similarities to STGD [25–27]. The physiopathological mechanism underlying this manifestation is still unclear. A possible role of subclinical inflammatory processes has been suggested for RP [28, 29] but not for STGD. On the other hand, in our series, a retinal surface structural re-arrangement could be related to photoreceptor atrophy within a more severe clinical picture. It should be noted that ef-OCT provides a bi-dimensional front view of the retinal surface, allowing better visualization of the morphology and extent of vitreo–retinal abnormalities.

The photoreceptor slab highlighted in all the STGD patients a central hypo-reflective area related to the disappearance of the ellipsoid zone of the photoreceptors. This may be considered a marker of photoreceptor degeneration, which is the core of STGD disease. These images could be useful to further process and quantify the extent and progression of retinal degeneration. In most of the cases (40/64 eyes, 63 %), limited hyper-reflective structures can be seen within the larger hypo-reflective area. Their interpretation is uncertain and they might be related to fibrotic processes, deposition of degenerative debris or surviving groups of photoreceptors.

Similarly, the above-RPE slab showed in all the eyes a central hypo-reflective area, less defined and homogeneous, however, than the corresponding alterations detected with the photoreceptor slab modality, probably because a thicker retinal slice included not only the photoreceptor layer but also the data originating from other contiguous outer-retina structures.

In some cases, some hyper-reflective structures can be seen within the larger hypo-reflective area, and probably correspond to the similar findings identified using the photoreceptor slab. Using the above RPE slab, they can be identified in fewer cases than in the photoreceptor slab. This is probably related to a higher thickness of the above RPE slab which is less capable of detecting very thin structures. In a few cases, these hyper-reflective structures show a spoke-like appearance, probably somehow related to the radial structure of Henle fibers and Muller cells.

The small hyper-reflective structures surrounding the central hypo-reflective abnormality are probably related to flecks. In fact, they can be seen in eyes where flecks are evident using funduscopy or auto-fluorescence (Fig. 11), and, moreover, their appearance using ef-OCT corresponds to the imaging of traditional SD-OCT where the flecks appear as localized RPE dome-shaped thickening. In a few cases, flecks could not be seen using ef-OCT with the above-RPE slab because they were located outside the area investigated by the OCT macular cube.

The RPE scan pointed out more or less homogeneous, central, hypo-reflective alterations related to RPE atrophy in 25/64 eyes (39 %). In some patients, these alterations could not be clearly detected, even in eyes where ~~a~~ macular RPE atrophy could be seen using funduscopic and auto-fluorescence imaging. This poor sensitivity may be due to the automatic procedure used by the Cirrus OCT software to process the data. In fact, with this visualization, the retinal slice is very thin (only

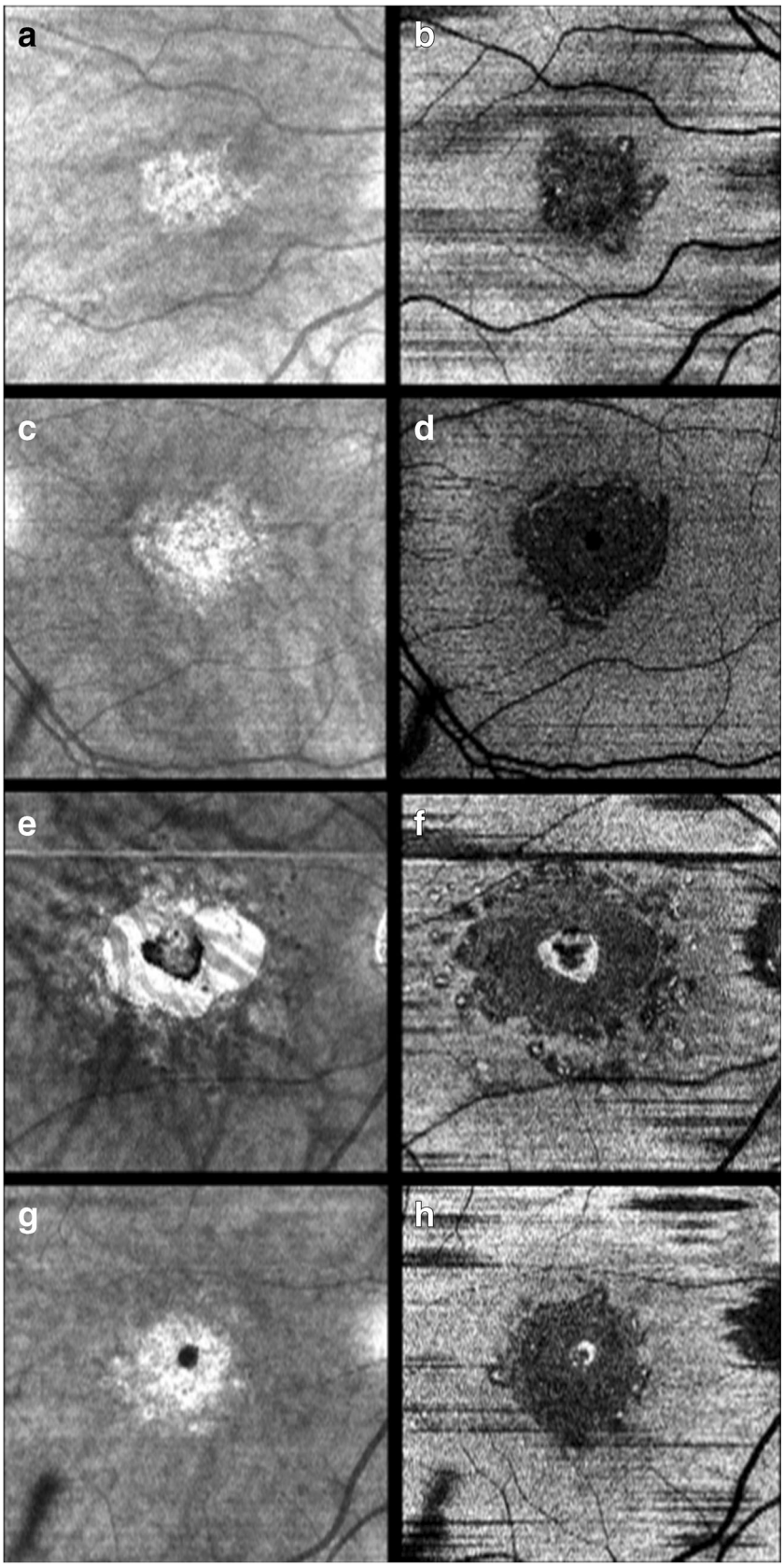

Fig. 10 (**a**, **b**, **c**, **d**, **e**, **f**, **g**, **h**): Comparison of the sub-RPE slab (**a**, **c**, **e**, **g**) and photoreceptor slab (b, d, f, h) of four patients; the area of photoreceptor atrophy exceeds that of the RPE atrophy. (**a**, **b**) Male patient, 51 years, right eye, BCVA of 20/200; (**c**, **d**) Male patient, 43 years, left eye, BCVA of 20/100; (**e**, **f**) Female patient, 53 years, right eye, BCVA of 20/400; (**g**, **h**) Male patient, 43 years, right eye, BCVA of 20/100

2 μm in comparison with the 10 μm attributed to the RPE layer thickness) and the automatic segmentation process may not fit the real profile of the RPE at the posterior pole correctly, especially in STGD eyes where

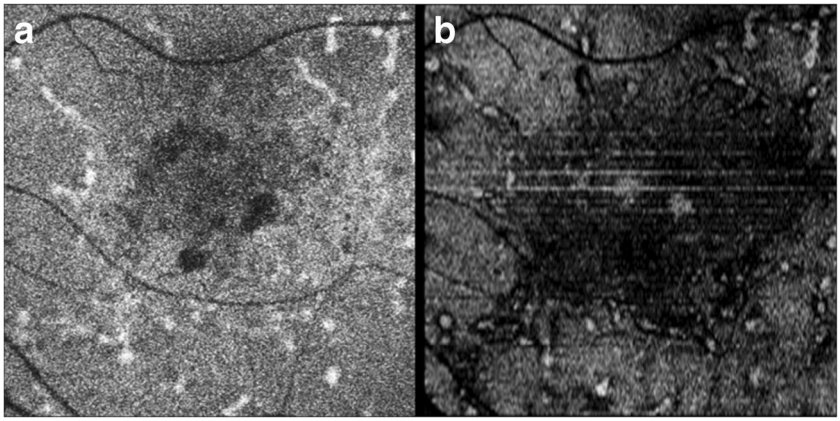

Fig. 11 (**a**, **b**): Comparison of autofluorescence imaging (**a**) and en face OCT above-RPE slab (**b**) in a female STGD patient, 68 years, left eye, BCVA of 20/400. The small hyper-reflective structures surrounding the central hypo-reflective abnormality are probably related to flecks.

the normal RPE is disrupted. Therefore, our results do not advise the regular use of this automatic OCT visualization procedure to evaluate the degree of RPE degeneration in STGD.

The sub-RPE slab could be more informative. A central hyper-reflective area determined by the light passing through atrophic RPE into the underlying choroid can be seen in 58/64 eyes (90.6 %) of 29 patients. The hyper-reflective area shows a high contrast in comparison with the surrounding choroid and allows an indirect but clear visualization of the extent and shape of central RPE atrophy. In particular, the alterations detected using the sub-RPE approach cannot be identified in the eyes where there was no significant RPE macular atrophy using fundoscopy (Fig. 12). In cases with geographic atrophy, the hyper-reflective area corresponded to the hypo-fluorescent areas detected using auto-florescence imaging (Fig. 13). In almost all the patients, where the comparison was possible, the extension of RPE atrophy (evaluated by means of the sub-

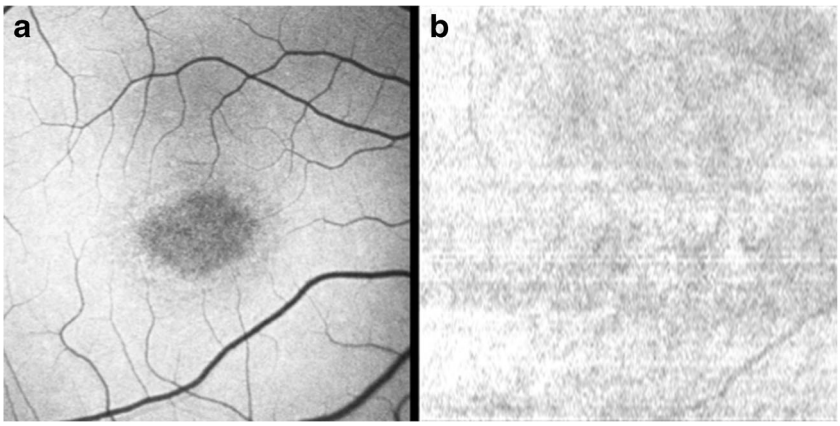

Fig. 12 (**a**, **b**): Comparison of autofluorescence imaging (**a**) and en face OCT sub-RPE slab (**b**) in the right eye of a female patient where there was no significant RPE macular atrophy; 10 years, BCVA of 20/100

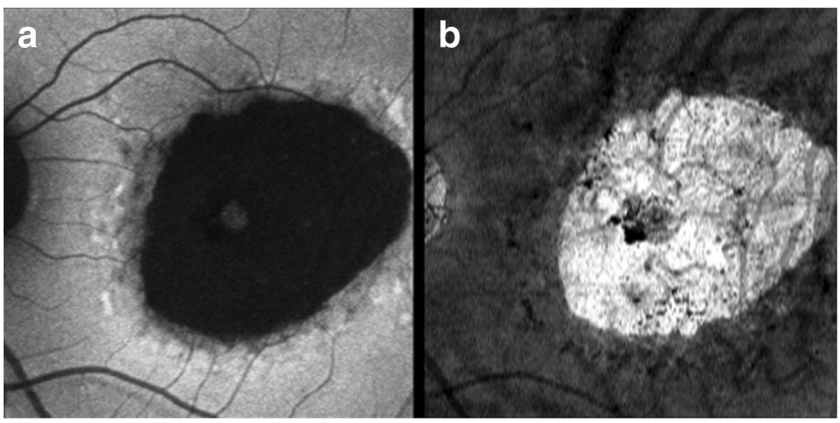

Fig. 13 (**a**, **b**): Comparison of macular atrophy evaluated with autofluorescence imaging (**a**) and en face OCT Sub-RPE slab (**b**) showing an evident correspondence of shape and extension of the lesion with both imaging modalities. Female patient, 54 years, BCVA of 20/400.

RPE slab) was noticeably exceeded by the extension of the photoreceptor atrophy (evaluated by means of the photoreceptor slab), suggesting that in STGD photoreceptor alterations predate RPE atrophy. Similar results have already been reported in atrophic age-related macular degeneration (AMD), supporting the hypothesis that photoreceptor disruption may represent an early defect leading to geographic atrophy (GA) [19]. These data are consistent with a possible sequence of the degenerative process in STGD, starting with storage of toxic metabolites, leading first to photoreceptor degeneration, then shedding of the photoreceptor disks phagocytized by the RPE with final atrophy of the RPE itself. This hypothesis is in agreement with a previous study showing photoreceptor alterations on OCT, without an equivalent abnormality with autofluorescence imaging, in some STGD patients [30].

In conclusion, ef-OCT proved to be a clinically useful tool for the management of STGD patients, illustrating in vivo the structural abnormalities of the different retinal layers. In particular, it images with great evidence vitreo-retinal interface alterations and the features of RPE and photoreceptor atrophy. Hopefully, the extent of atrophic processes may be further evaluated with computer-assisted analysis providing measurable parameters related to the progression of retinal degeneration. In STGD, ef-OCT may allow a better understanding of the physiopathology of the disease and a reliable monitoring of disease progression and possible response to innovative therapeutic strategies.

Compliance of ethical standards All procedures performed in studies involving human participants were in accordance with the ethical standards of the institutional and/or national research committee and with the 1964 Helsinki declaration and its later amendments or comparable ethical standards.

Conflict of Interest All authors certify that they have no affiliations with or involvement in any organization or entity with any financial interest (such as honoraria; educational grants; participation in speakers' bureaus; membership, employment, consultancies, stock ownership, or other equity interest; and expert testimony or patent-licensing arrangements), or non-financial interest (such as personal or professional relationships, affiliations, knowledge or beliefs) in the subject matter or materials discussed in this manuscript.

Informed consent Informed consent was obtained from all individual participants included in the study.

Funding No funding was received for this research.

References

1. Walia S, Fishman GA, Kapur R (2009) Flecked-retina syndromes. Ophthalmic Genet 30(2):69–75
2. Sodi A, Bini A, Passerini I, Forconi S, Menchini U, Torricelli F (2010) Different patterns of fundus autofluorescence related to ABCA4 gene mutations in Stargardt disease. Ophthalmic Surg Lasers Imaging 41(1):48–53
3. Testa F, Rossi S, Sodi A et al. (2012) Correlation between photoreceptor layer integrity and visual function in patients with Stargardt disease: implications for gene therapy. Invest Ophthalmol Vis Sci. 3; 53(8): 4409–15.
4. Lois N, Holder GE, Bunce C, Fitzke FW, Bird AC (2001) Phenotypic subtypes of Stargardt macular dystrophy-fundus flavimaculatus. Arch Ophthalmol 119(3):359–69
5. Fujinami K, Lois N, Davidson AE, Mackay DS, Hogg CR, Stone EM, Tsunoda K, Tsubota K, Bunce C, Robson AG, Moore AT, Webster AR, Holder GE, Michaelides M (2013) A longitudinal study of stargardt disease: clinical and electrophysiologic assessment, progression, and genotype correlations. Am J Ophthalmol 155(6):1075–1088.e13
6. Allikmets et al (1997) A photoreceptor cell-specific ATP-binding transporter gene (ABCR) is mutated in recessive Stargardt macular dystrophy. Nat Genet 15(3):236–46
7. Passerini I, Sodi A, Giambene B et al (2010) Novel mutations in of the ABCR gene in Italian patients with Stargardt disease. Eye (Lond) 24(1):158–64
8. Cideciyan AV, Aleman TS, Swider M et al (2004) Mutations in ABCA4 result in accumulation of lipofuscin before slowing of the retinoid cycle: a reappraisal of the human disease sequence. Hum Mol Genet 13(5):525–34
9. Radu RA, Yuan Q, Hu J et al (2008) Accelerated accumulation of lipofuscin pigments in the RPE of a mouse model for ABCA4-mediated retinal dystrophies following Vitamin A supplementation. Invest Ophthalmol Vis Sci 49(9):3821–9
10. Han Z, Conley SM, Naash MI (2014) Gene therapy for Stargardt disease associated with ABCA4 gene. Adv Exp Med Biol 801:719–24
11. Auricchio A, Trapani I, Allikmets R (2015) Gene Therapy of ABCA4-Associated Diseases. Cold Spring Harb Perspect Med 8: 5(5)
12. Van Velthoven ME, de Vos K, Verbraak FD, Pool CW, de Smet MD (2005) Overlay of conventional angiographic and en-face OCT images enhances their interpretation. BMC Ophthalmol 5:12
13. Van Velthoven ME, Verbraak FD, Yannuzzi LA, Rosen RB, Podoleanu AG, de Smet MD (2006) Imaging the retina by en face optical coherence tomography. Retina 26(2):129–36
14. Forte R, Pascotto F, de Crecchio G (2007) Visualization of vitreomacular tractions with en face optical coherence tomography. Eye (Lond) 21(11):1391–4
15. Forte R, Cennamo G, Pascotto F, de Crecchio G (2008) En face optical coherence tomography of the posterior pole in high myopia. Am J Ophthalmol 145(2):281–288
16. Kameda T, Tsujikawa A, Otani A, Sasahara M, Gotoh N, Tamura H, Yoshimura N (2007) Polypoidal choroidal vasculopathy examined with en face optical coherence tomography. Clin Experiment Ophthalmol 35(7):596–601
17. Rispoli M, Le Rouic JF, Lesnoni G, Colecchio L, Catalano S, Lumbroso B (2012) Retinal surface en face optical coherence tomography: a new imaging approach in epiretinal membrane surgery. Retina 32(10):2070–6
18. Adhi M, Liu JJ, Qavi AH, Grulkowski I, Fujimoto JG, Duker JS (2013) Enhanced visualization of the choroido-scleral interface using swept-source OCT. Ophthalmic Surg Lasers Imaging Retina 44(6 Suppl):S40–2
19. Nunes RP, Gregori G, Yehoshua Z et al (2013) Predicting the progression of geographic atrophy in age-related macular degeneration with SD-OCT en face imaging of the outer retina. Ophthalmic Surg Lasers Imaging Retina 44(4):344–59
20. Yehoshua Z, Garcia Filho CA, Penha FM et al (2013) Comparison of geographic atrophy measurements from the OCT fundus image

and the sub-RPE slab image. Ophthalmic Surg Lasers Imaging Retina 44(2):127–32
21. Mazzini C, Sodi A, Menchini U. (2013) En face optical coherence tomography in retinal dystrophies. In Bruno Lumbroso (ed), David Huang (ed), Andre Romano (ed) Clinical En Face OCT Atlas First edition, Jaypee brother medical publishers. Printed at: Ajanta Offset & Packagings Ltd New Delhi.
22. Spaide RF, Curcio CA (2011) Anatomical correlates to the bands seen in the outer retina by optical coherence tomography: literature review and model. Retina 31(8):1609–19
23. Yehoshua Z, Garcia Filho CA, Penha FM, Gregori G, Stetson PF, Feuer WJ, Rosenfeld PJ (2013) Comparison of geographic atrophy measurements from the OCT fundus image and the sub-RPE slab image. Ophthalmic Surg Lasers Imaging Retina 44(2):127–32
24. Sodi A, Bini A, Passerini I, Menchini U, Torricelli F (2006) Occurrence of full-thickness macular hole complicating Stargardt disease with ABCR mutation. Eur J Ophthalmol 16(2):335–8
25. Jin ZB, Gan DK, Xu GZ, Nao-I N (2008) Macular hole formation in patients with retinitis pigmentosa and prognosis of pars plana vitrectomy. Retina 28(4):610–4
26. Hagiwara A, Yamamoto S, Ogata K, Sugawara T, Hiramatsu A, Shibata M, Mitamura Y (2011) Macular abnormalities in patients with retinitis pigmentosa: prevalence on OCT examination and outcomes of vitreoretinal surgery. Acta Ophthalmol 89(2):e122–5
27. Testa F, Rossi S, Colucci R et al (2014) Macular abnormalities in Italian patients with retinitis pigmentosa. Br J Ophthalmol 98(7): 946–50
28. Yoshida N, Ikeda Y, Notomi S et al (2013) Laboratory evidence of sustained chronic inflammatory reaction in retinitis pigmentosa. Ophthalmology 120(1):e 5–e 12
29. Murakami Y, Yoshida N, Ikeda Y et al (2015) Relationship between aqueous flare and visual function in retinitis pigmentosa. Am J Ophthalmol 159(5):958.e1–963.e1
30. Gomes NL, Greenstein VC, Carlson JN et al (2009) A comparison of fundus autofluorescence and retinal structure in patients with Stargardt disease. Invest Ophthalmol Vis Sci 50(8):3953–9